frontiers | Frontiers in Nanotechnology

TYPE Original Research
PUBLISHED 11 August 2025
DOI 10.3389/fnano.2025.1631560

OPEN ACCESS

EDITED BY
Zeinab Ramezani,
University of Miami, United States

REVIEWED BY
V. Mahendran,
Institut Jožef Stefan (IJS), Slovenia
Mohsen Mahmoudysepehr,
University of Waterloo, Canada

*CORRESPONDENCE
M. Cecilia Fuertes,
cecilia.fuertes@conicet.gov.ar

RECEIVED 19 May 2025
ACCEPTED 25 July 2025
PUBLISHED 11 August 2025

CITATION
Morrone J, Angelomé PC, Zelcer A and Fuertes MC (2025) Selective functionalization of mesoporous UV photonic crystals for the detection of organic vapors.
Front. Nanotechnol. 7:1631560.
doi: 10.3389/fnano.2025.1631560

Selective functionalization of mesoporous UV photonic crystals for the detection of organic vapors

Josefina Morrone [1], Paula C. Angelomé [1], Andrés Zelcer [2] and M. Cecilia Fuertes [1,3]*

[1]Gerencia Química & INN, Centro Atómico Constituyentes, Comisión Nacional de Energía Atómica, San Martín, Buenos Aires, Argentina, [2]CIBION, CONICET, Ciudad Autónoma de Buenos Aires, Argentina & ECyT, Universidad Nacional de San Martín, San Martín, Buenos Aires, Argentina, [3]Instituto Sabato, Comisión Nacional de Energía Atómica – Universidad Nacional de San Martín, San Martín, Buenos Aires, Argentina

Mechanically robust and chemically stable responsive photonic crystals (PC), featuring a photonic band gap centered in the UV region and exhibiting very high reflectivities, were fabricated by alternate deposition of mesoporous zirconia and silica thin films. These multilayered structures were synthesized via dip-coating, using a sol-gel method combined with self-assembly of surfactants, to give rise to the mesoporosity, in which capillary condensation can take place. By exploiting the chemical differences between silicon and zirconium oxides, selective functionalization of the layers that compose the PC was achieved, as demonstrated by infrared spectroscopy, energy dispersive spectroscopy and contact angle measurements. Once obtained, the functionalized PC were tested for vapors detection using water and non-polar organic solvents. The obtained results indicate that water entrance within the PC can be hindered by the presence of organic functions, while organic solvents can be detected in any case. Thus, the selective functionalization strategy developed allows the precise control over the PC response toward analytes with varying physicochemical properties. Moreover, the band gap located in the UV region allows the combination of the developed PC with other sensing devices working in the visible region of the spectrum, paving the way towards the production of highly tunable sensor arrays.

KEYWORDS

photonic crystals, sol gel, optical detectors, functionalization, silica, zirconia, mesoporous films, responsive devices

Introduction

As contamination of air, water, and soil increases, there is a pressing demand for accurate and efficient monitoring and detection of harmful substances, driving the development of advanced sensing platforms capable of providing rapid, sensitive, and reliable responses to the presence of contaminants. In particular, optical sensors are widely employed to detect analytes and bacterial contaminants across various industries, including food, pharmaceutical, and chemical sectors (Fenzl et al., 2014; Paternò et al., 2019; Shen et al., 2022; Butt and Piramidowicz, 2024). Their operating principle relies on measuring

how light interacts with matter, enabling the detection of changes in physical, chemical, or biological properties.

Responsive photonic crystals represent a promising strategy for the development of optical sensors (Burgess et al., 2013; Xu et al., 2013; Musgrove et al., 2024; Wei et al., 2024). Photonic crystals (PCs) are material systems with a periodically varying refractive index. This modulation of the dielectric function alters light propagation, leading to the selective reflection of a specific range of wavelengths, known as the photonic band gap (Joannopoulos et al., 2011). The simplest PCs are those in which the refractive index is periodically modulated in only one direction (one-dimensional photonic crystals, 1D-PC). These devices are built by stacking layers with different thicknesses and refractive indices. The position and intensity of the photonic band gap can be tuned by adjusting the layer thicknesses and/or their effective refractive indices. The working principle of these 1D-PC sensors is based on the fact that any changes in the refractive index contrast between layers or in the layer thicknesses alters the optical properties. Thus, when either of these two parameters changes in response to an external stimulus, the system exhibits a detectable optical modification (Däntl et al., 2022).

In addition, the development of responsive PCs with a reflective band gap in the UV (UV-PC) range offers the possibility of integrating them with other sensing platforms that operate in the visible range, avoiding spectral overlap and enabling simultaneous detection of multiple analytes through distinct spectral windows. The materials used to construct responsive UV-PC must be transparent in the UV region, exhibit a significant refractive index contrast that changes when exposed to analytes, and be resistant to water vapor. Besides, a reproducible and controlled synthesis method must be available to produce thin films with well-controlled thickness in the appropriate range to tune the position of the photonic band gap. Ceramic mesoporous thin films are excellent building blocks to prepare PCs responsive to organic vapors since, in contrast to polymeric materials, they do not swell and deform upon solvent exposure and are resistant to UV radiation.

Optical detectors based on mesoporous oxide films synthesized using the sol-gel method have gained increasing global attention over the past decade due to the simplicity and versatility of their synthesis, as well as their robustness, chemical and mechanical stability, and reproducible preparation (Fuertes et al., 2007; Ghazzal et al., 2012a; Sansierra et al., 2019; Ramallo et al., 2022; Morrone et al., 2023). The sequential deposition of these thin films enables the fabrication of responsive 1D-PCs. When the mesoporous films are integrated into a PC, analytes can diffuse into the layers through the high accessible porosity, altering the average refractive index and producing a measurable optical response. In particular, due to the characteristic pore size (2–50 nm), vapor analytes undergo capillary condensation within the pores, leading to significant changes in the effective refractive index of each porous layer. As a result, a shift in the position and intensity of the photonic band gap is observed (Choi et al., 2006; Fuertes et al., 2007; Sansierra et al., 2019). These devices are especially attractive because of their reversible optical response. However, challenges remain in improving responsiveness toward specific molecules and minimizing interference from water condensation in ambient environments, which are critical factors that must be addressed during sensor design.

The selectivity of these optical detectors is, in the first place, influenced by their structural features and can be enhanced by controlling analytes diffusion within the mesoporous multilayer. This diffusion is primarily governed by the size of the pores and necks, as well as their geometric arrangement (Fuertes et al., 2008; López-Puente et al., 2015). When considering only their structural characteristics, these materials exhibit poor selectivity, as nearly any small analyte can diffuse through the multilayer. Therefore, enhancing selectivity by tuning the physicochemical properties of the system is essential. This can be achieved through the use of hybrid materials, such as inorganic oxides modified with organic functions (Athens et al., 2009) or metal-organic frameworks (Hinterholzinger et al., 2012; Shen et al., 2022; Wang et al., 2022). In particular, hybrid organic-inorganic mesoporous oxides thin films can be prepared either by incorporating a small proportion of an organic component during the synthesis of the oxide (Nicole et al., 2005) or by post-functionalizing the devices through various chemical reactions (Fuertes et al., 2007; Ghazzal et al., 2012a).

This PC functionalization strategy was proven to be successful to distinguish different chemical species in liquid and vapor phases. In particular, it has been demonstrated the feasibility of using silanes to modify the surface of SiO_2 nanoparticles by post functionalization to generate responsive photonic noses with differential sensitivity to organic vapors and bacteria (Bonifacio et al., 2010; Bonifacio et al., 2011). However, these systems are based on SiO_2 and TiO_2 nanoparticles and, consequently, the photonic band gap of the resulting PC cannot be centered in the UV region due to the strong UV absorption of TiO_2. Besides, nanoparticle-based PC generally exhibit limited mechanical stability and poor adhesion to the substrate (Jeong et al., 2025). As a result, polymeric binders are often required to consolidate the structure, which can compromise their responsiveness (Meng et al., 2024). In contrast, PC fabricated using sol–gel-derived mesoporous thin films are mechanically robust and well-adhered and can be handled and exposed to vapors or liquids without losing their structural integrity or sensing performance (Ramallo et al., 2022; Morrone et al., 2023).

Silanes were also used to produce functional mesoporous SiO_2 films, which were successfully combined with mesoporous TiO_2 films to construct PCs. In this case, a difference between the sensitivity towards liquids with different polarities as a function of the functionalization degree was demonstrated (Ghazzal et al., 2012b). In addition, the use of transition metal complexing agents to impart selectivity in PCs based on TiO_2 and SiO_2 mesoporous thin films was also demonstrated, again in the liquid phase (Fuertes et al., 2007). Interestingly, the sensitivity of these functional PCs was not demonstrated in vapor phase and their photonic band gap is restricted to the visible–NIR spectral range.

In this work, the differential functionalization of mesoporous oxide UV-PC was studied, as a means to tune the selectivity of the detector in the vapor phase and to limit the condensation of water vapor into the mesopores. Silica and zirconia were selected to construct the PC with the band gap in the UV region of the spectrum. These oxides were chosen for their transparency in the UV range, their chemical and mechanical robustness, and highly reproducible and simple synthesis. Moreover, the significant refractive index contrast allows the construction of a highly reflective UV-PC with few layers. Additionally, their surface

chemistries differ; to take advantage of this, zirconia layers were modified through complexation with transition metal oxide complexing agents (Angelomé and Soler-Illia, 2005; Fuertes et al., 2007), while silica layers were selectively functionalized via silanization (Zhao and Lu, 1998; Venkateswara Rao et al., 2009; Sun et al., 2021). Functionalization strategies minimize the access of ambient water vapor into the porous multilayers and enhance the responsiveness to non-polar vapors. The obtained devices were tested as selective non-polar vapors detectors by monitoring static and dynamic changes in the position of the PCs band gap.

Materials and methods

Materials

Tetraethoxysilane (TEOS), Pluronic F127 ($[EO]_{106}$ $[PO]_{70}$ $[EO]_{106}$; EO = ethylene oxide, PO: propylene oxide), cetyltrimethylammoniumbromide (CTAB), acetylacetone (ACAC), dihexadecyl phosphate (DHDP), and chlorotrimethylsilane (TMCS) were supplied by Sigma-Aldrich. Zirconium isopropoxide ($Zr(OCH_2CH_2CH_3)_4$), N,N-diisopropylethylamine (DIPEA), benzyl alcohol, and hydrochloric acid were purchased from Merck. Ethanol was purchased from Cicarelli. Tetrahydrofurane (THF) was supplied by Biopack, and toluene by Anedra. E-pure water (18 MΩ.cm) was used as a reagent.

Sols, films and multilayers preparation

Mesoporous oxide thin films were deposited by dip coating on glass substrates, combining the sol-gel process and evaporation induced self-assembly of surfactants (Brinker et al., 1999).

For the production of mesoporous SiO_2 films (named SC), a prehydrolysis solution was formulated by refluxing TEOS for 1 h in a water-ethanol solution, with $[H_2O]$:[Si] = 1 and [EtOH]:[Si] = 5. SC films were obtained with the sol comprised of TEOS:CTAB:H_2O:EtOH:HCl with a molar ratio 1:0.1:5:40:0.004. Mesoporous silica films synthesized using this surfactant exhibit an ordered and interconnected pore array with three-dimensional hexagonal ($P6_3/mmc$) structure, with a characteristic pore diameter of around 3 nm (Fuertes et al., 2008).

On the other hand, a solution containing $Zr(OCH_2CH_2CH_3)_4$:F127:H_2O:EtOH:HCl:ACAC with molar ratios 1:0.005:20:40:1:1 was used for deposition of mesoporous ZrO_2 films (named ZF). The mesoporous zirconia films synthesized using this surfactant usually present ordered arrangements of pores in an Im3m cubic structure, with pore diameters between 8 and 10 nm (Zelcer and Soler-Illia, 2013).

Three different types of samples were prepared: single-layer films, bilayer films, and PCs. The single-layer SC and ZF films were deposited onto bare glass by dip-coating. The deposition was carried out using an extraction speed of 2 mm/s, and was performed in an environment with a relative humidity (RH) of 20%. This extraction speed was chosen in order to obtain thick films that are more appropriate for studying functionalization effects, as they provide a larger amount of material and surface area for interaction with functionalization agents and analytes. SC samples were thermally treated for 30 min periods at room temperature, 60 °C, 130 °C and 200 °C; ZF films were treated directly at 200 °C also for 30 min (Zelcer and Soler-Illia, 2013). These thermal treatments consolidate the films, but are mild enough to preserve the surfactants inside the pores. Therefore, a new layer can be deposited on top of these films without filling the mesopores with the precursor solution (Fuertes et al., 2007).

TABLE 1 Description of the evaluated systems and their corresponding nomenclature.

Sample	Multilayer	Functionalizing agent
PC	4X (SC/ZF)	-
PC-TMCS	4X (SC/ZF)	TMCS
PC-DHDP	4X (SC/ZF)	DHDP
PC-TMCS + DHDP	4X (SC/ZF)	1st) TCMS 2nd) DHDP

For bilayers, successive deposition of SC and ZF layers was carried out following alternating steps of deposition and thermal treatment for each material. Both possible material order configurations were built, with either the SC film or the ZF film adjacent to the substrate. To remove the surfactant, the same treatment was applied to all systems: the samples were heated to 350 °C with a temperature ramp of 1 °C/min, and held at that temperature for 2 h.

In the case of the PCs, alternating deposition of the SC and ZF mesoporous oxide layers by dip-coating was performed with extraction speeds of 1 mm/s. This extraction speed was selected to obtain layer thicknesses that yield a device with a photonic band gap in the UV region of the spectrum. The same thermal treatments used for the single and bilayers were applied to the PCs. However, in this case, fused silica was used as a substrate since this substrate is transparent in the UV, the range of the electromagnetic in wich the photonic band gap is expected to be located. The synthesized photonic crystals were named 4X (SC/ZF), where 4 represents the number of bilayers deposited and the films that comprise each one of them are indicated in parenthesis, being the silica film the one adjacent to the substrate.

A flowchart showing the steps involved in the preparation of single layers, bilayers and PCs is presented in Supplementary Figure S1.

Post-synthesis modification

Mesoporous systems were functionalized using TMCS and DHDP. TMCS acts as a silanizing agent for SiO_2, reacting with surface silanol groups to form $OSi(CH_3)_3$ species (Zhao and Lu, 1998; Venkateswara Rao et al., 2009; Sun et al., 2021). In contrast, DHDP anchors to transition metals by surface complexation (Angelomé and Soler-Illia, 2005). A scheme of the functionalization reactions is presented in Supplementary Figure S2.

To perform the silanization, the samples were first cleaned with ethanol, dried, and then immersed for 10 min in a 9% w/w solution of TMCS in toluene. To accelerate the functionalization reaction, a few drops of DIPEA were added to the solution. Functionalization with DHDP was carried out by immersing the samples in a 0.01 M

DHDP solution in THF. For single and bilayer samples, the immersion time was 2 h, following previously established protocols (Angelomé and Soler-Illia, 2005; Fuertes, 2009). In the case of multilayer systems, the immersion time was extended to 24 h to ensure uniform functionalization throughout the porous network. When dual functionalization was required, TMCS modification was performed prior to DHDP functionalization, in order to avoid the potential removal of DHDP molecules by toluene. A flowchart showing the steps involved in the functionalization of the PCs is presented in Supplementary Figure S3. The nomenclature adopted for the multilayers analyzed in this study is summarized in Table 1.

TABLE 2 Contact angle (CA) values, thickness, and water-accessible porosity (P_A) of SC and ZF single layers before and after functionalization with TMCS or DHDP.

Sample	CA/°	Thickness/nm	P_A/%
SC	44 ± 2	100 ± 10	38 ± 4
SC – TMCS	89 ± 1	100 ± 10	12 ± 2
SC – DHDP	51 ± 2	100 ± 10	33 ± 3
ZF	21 ± 4	91 ± 9	30 ± 3
ZF – TMCS	54 ± 2	90 ± 9	22 ± 2
ZF – DHDP	59 ± 2	95 ± 9	11 ± 2

Characterization

Porosity and thickness were determined using X-ray reflectometry (XRR) with a Panalytical Empyrean X-ray diffractometer and CuK_α incident radiation (λ = 1.54 Å) (van der Lee, 2000). A specially designed chamber was used to control the RH in the sample environment in order to obtain the porosity. A full description of the method can be found elsewhere (Fuertes et al., 2009; Steinberg et al., 2019).

Infrared spectroscopy was used to characterize the chemical modifications introduced by surface functionalization. Measurements were performed using NICOLET Magna 560 or NICOLET 8700 instruments equipped with liquid N_2 cooled MCT-A detectors. Transmission mode was employed to acquire spectra of samples deposited on glass or fused silica substrates in the 3,500–2,500 cm^{-1} range. In this case, the samples were directly mounted onto the sample holder. Diffuse reflectance mode (Diffuse reflectance infrared Fourier transform spectroscopy, DRIFTS), on the other hand, was used to determine the samples full spectra (4,000–600 cm^{-1} range). In this case, the samples were scratched from the substrate and mixed with KBr to perform the measurements.

Modifications in the hydrophobicity of the synthesized materials were determined by liquid-solid contact angle (CA) measurements. A Ramé-Hart 290 equipment was used, and the acquired images were processed with DROPimage Advanced V25 software. All samples were dried at 130 °C before each measurement.

The multilayer structure and chemical composition before and after post-synthesis modifications was characterized by transmission electron microscopy (TEM) coupled with Energy Dispersive Spectroscopy (EDS), using a Philips CM 200 microscope operated at an accelerating voltage of 180 kV coupled with an EDAX® detector. Samples were prepared by scratching the photonic crystals and dispersing the resulting fragments onto carbon-coated copper grids.

Sensing performance

The performance of the different photonic crystals as optical devices for the detection of non-polar organic vapors was evaluated. The transmission spectra of the multilayer systems were measured by UV-visible spectroscopy using an Agilent 8453 diode array spectrophotometer. Measurements were taken on samples subjected to a low RH atmosphere (dry conditions, between 5% and 10% RH) and in a H_2O (n_{630} = 1.333; P_v = 15.7 kPa at 55 °C, being n_{630} the refractive index at λ = 630 nm and P_v the vapor pressure) (Sienko and Plane, 1967; Haynes, 2003) saturated atmosphere, and exposed to organic solvents saturated atmospheres. Measurements were carried out both under static equilibrium conditions and dynamically at regular time intervals, to evaluate the response kinetics in environments containing either pure vapor solvents or mixtures of polar and non-polar solvents. The organic solvents used were toluene (n_{630} = 1.496; P_v = 15.3 kPa at 55 °C) and benzyl alcohol (n_{630} = 1.540; P_v = 0.13 kPa at 55 °C). These organic compounds were selected because they exhibit similar refractive indices but markedly different vapor pressures and physicochemical properties. Water was included to assess the impact of ubiquitous ambient humidity on the device response. Prior to use, the organic solvents were dried using 3A and 4A molecular sieves.

The performance was evaluated by analyzing the response times for each pure solvent and for the solvents' mixture, defined as the minimum time in which the greatest shift of the photonic band gap (λ_B) is reached (Sansierra, 2019). To carry out the experiments, the samples were placed inside a quartz cuvette mounted in a sample holder at 55 °C. For the pure solvent tests, a filter paper soaked with the solvent of interest was placed inside the cuvette. In the case of solvent mixtures, two filter papers were introduced simultaneously, one imbibed with water and the other with the non-polar solvent. Prior to each experiment, the samples were rinsed with ethanol and dried in an oven at 130 °C for 10 min to ensure the complete removal of the solvents and water from the mesopores.

Results and discussion

Chemical and structural features

Single-layers and bilayers characterization

Single and bilayer mesoporous systems were synthesized, subjected to different post-synthesis modifications, and their chemical nature, wettability and accessible porosity was evaluated by different techniques.

Film thicknesses were determined by XRR. For all layers, the thicknesses estimated from the Kiessig fringes are approximately 90–100 nm in both single layers and for each layer forming the bilayer structure. These relatively thick films enable the acquisition of good DRIFTS signals and allow CA measurements to be

10.3389/fnano.2025.1631560

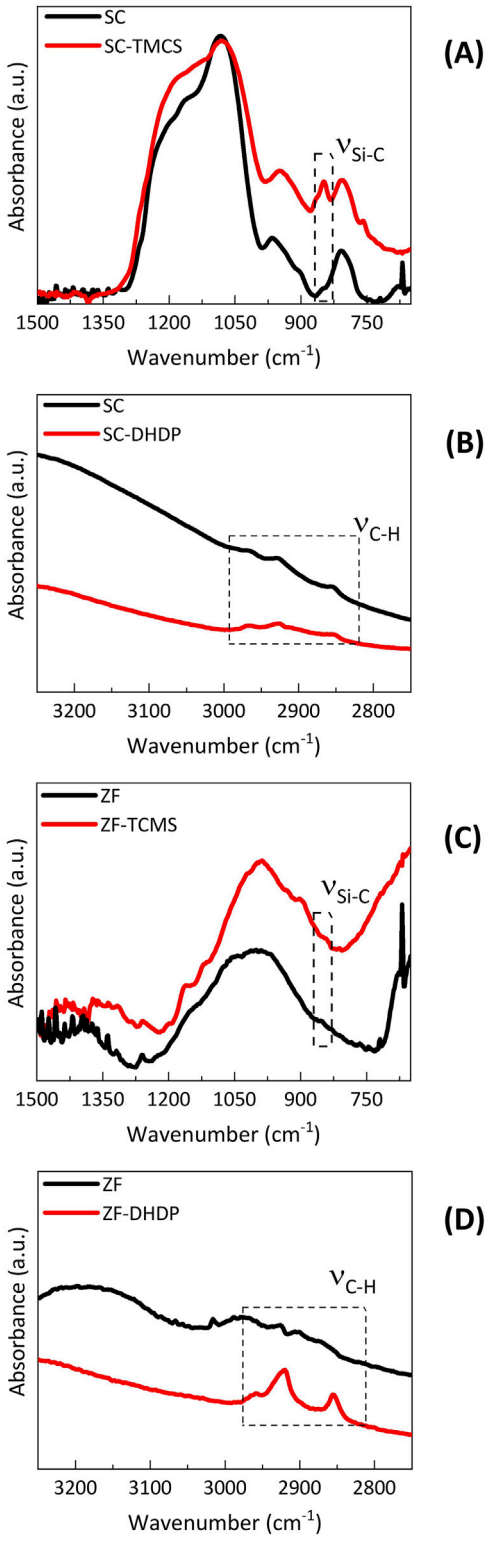

FIGURE 1
DRIFTS spectra of SC and ZF films: **(A)** SC before (black) and after (red) functionalization with TMCS; **(B)** SC before (black), and after (red) functionalization with DHDP; **(C)** ZF before (black) and after (red) functionalization with TMCS; **(D)** ZF before (black), and after (red) functionalization with DHDP.

performed with reduced influence from substrate effects. No significant changes in thickness are observed after the chemical modifications in either oxide (Table 2).

Chemical modifications were studied using DRIFT spectroscopy. The regions of interest for the two tested chemical functions are between 1,500 and 650 cm^{-1} for TMCS, and around 2,900 cm^{-1} for DHDP. Figure 1 shows these selected regions of the spectra of SC films and ZF films before and after reacting with each of these molecules. After functionalization with TMCS, SC films spectra (Figure 1A) show a new absorption band at 850 cm^{-1} due to the Si-C stretching vibration (ν_{Si-C}) (Sun et al., 2021). On the contrary, functionalization of SC films with DHDP does not produce a significant change in the 3,000–2,800 cm^{-1} region, as shown in Figure 1B. Thus, TMCS effectively modifies the SiO_2 surface of these mesoporous films, while DHDP shows poor affinity for SC films. Figure 1C shows the IR spectra between 650 and 1,500 cm^{-1} of the ZF system before and after functionalization with TMCS. In this case, the characteristic band associated with ν_{Si-C} vibrations is not observed, indicating that TMCS does not anchor to this oxide. Nevertheless, after functionalization with DHDP (Figure 1D), bands corresponding to the C-H stretching vibrations (ν_{C-H}) of the alkyl chain are clearly visible (Angelomé and Soler-Illia, 2005). These results show that, for ZF films, DHDP acts as an effective surface functionalization agent, while TMCS does not bind to the material.

In conclusion, TMCS and DHDP can serve as selective functionalization agents for systems composed of SiO_2 and ZrO_2.

When analyzing the DRIFTS spectra of bilayer systems, it is not possible to determine which surface the functionalizing agents are attached to. After TCMS functionalization, the band between 650 and 1,500 cm^{-1} corresponding to the ν_{Si-C} vibrations appears in the IR spectra, as observed in both bilayer configurations: SC/ZF and ZF/SC (Supplementary Figure S4A,C). In the case of DHDP functionalization (Supplementary Figure S4B,D), the expected bands corresponding to the ν_{C-H} vibrations of the alkyl chain are clearly visible in the high wavenumber region. These results indicate that both functionalizing agents anchor to at least part of the surface of these complex systems. Although it is reasonable to assume that the selectivity observed for single-layer films also applies to bilayers, this technique does not provide direct evidence to confirm this.

The substitution of surface OH groups with hydrocarbon chains is expected to increase surface hydrophobicity. In the studied samples, the effect of functionalization on hydrophobicity was evaluated by measuring changes in the water contact angle (CA). Images of the films before and after functionalization, with a water droplet on their surface, are shown in Figure 2, and the corresponding CA values are presented in Table 2.

Functionalization with either agent leads to a significant increase in the hydrophobicity of both oxides. In the case of a single-layer SC mesoporous film, the water/film CA increases from 44° to 89° after functionalization with TMCS, whereas DHDP treatment results in only a modest increase to 51°. These findings are consistent with the DRIFTS results, which confirm that TMCS effectively attaches organic moieties to SC films. The DHDP functionalization process, which involves exposing the film to anhydrous

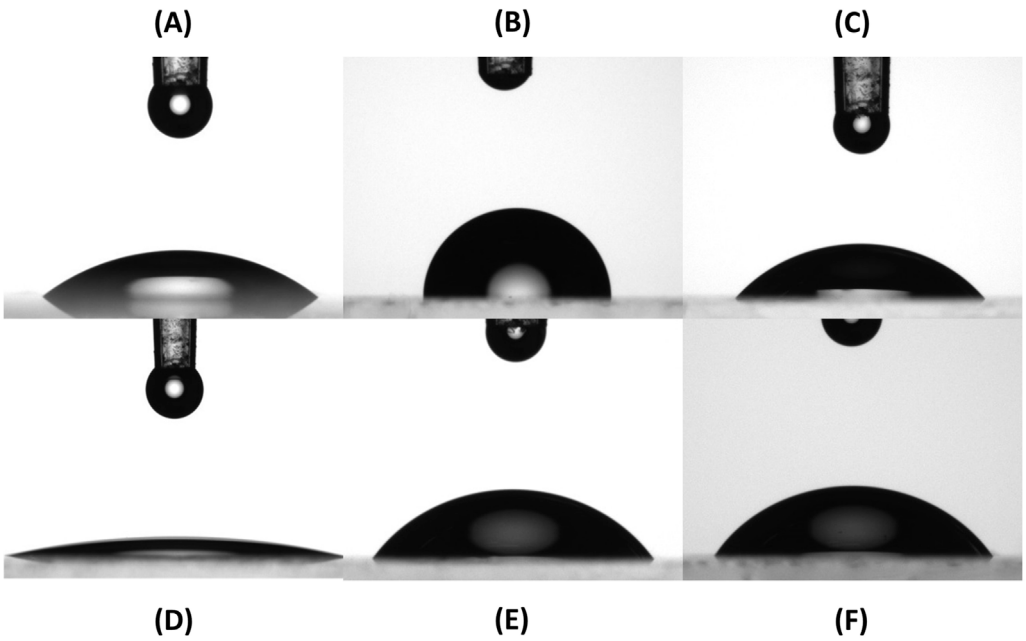

FIGURE 2
Images of water droplets deposited on SC **(A)**, SC-TMCS **(B)**, SC-DHDP **(C)**, ZF **(D)**, ZF-TMCS **(E)** and ZF-DHDP **(F)** systems from which the contact angles were determined.

conditions in the presence of an acid, may promote condensation of surface Si–OH groups, resulting in less hydrophilic surfaces and a corresponding increase in CA.

For single-layer mesoporous ZF films, the water CA of the as-prepared surface is 21°, increasing to 59° after DHDP functionalization and to 54° after reaction with TMCS. Unlike SC films, the increase in CA upon functionalization is less pronounced, and both chemical treatments produce a similar effect. Film wettability depends not only on the nature of the exposed functional groups but also on the polarizability of the material. Since ZrO_2 exhibits higher polarizability than SiO_2, the influence of surface modification is comparatively reduced. Additionally, TMCS acts as a strong dehydrating agent, promoting the condensation of vicinal Zr-OH groups and thereby decreasing surface hydrophilicity. This is supported by the shift of the broad OH band in the IR spectrum to higher wavenumbers, consistent with the disappearance of hydrogen-bonded OH groups. As a result of these combined effects, the CA values after functionalization with either reagent are similar.

Changes in the water CA of bilayer systems are primarily governed by the behavior of the top layer. Functionalization of the SC/ZF system with DHDP and TMCS leads to CA increases of 117% and 113%, respectively, indicating a marked enhancement in hydrophobicity. For the ZF/SC system, CA increases of 31% and 153% are observed upon treatment with DHDP and TMCS, respectively. These increases are comparable to those obtained for SC single-layers. In both bilayer configurations, it is important to note that although the top layer has a dominant effect on wettability, the underlying layer also contributes to the overall surface behavior (Fuertes et al., 2008).

Water-accessible porosities (P_A) were also determined by XRR. The P_A measurements are based on the capillary condensation of water within the mesopores of the films. The critical angle of total reflection (θ_C) obtained from XRR is directly related to the electron density of the material (van der Lee, 2000). By performing measurements at low RH, when the mesopores are empty, and at high RH, when capillary condensation occurs, the relative volume of the films accessible to water can be determined (Klotz et al., 2006).

Figure 3A shows the XRR measurements of SC films under low and high RH conditions. A pronounced shift in the critical angle is observed in the presence of water vapor for both non-functionalized and DHDP-functionalized films. In contrast, TMCS-treated films exhibit only a small shift in the critical angle. The P_A values derived from these shifts are presented in Table 2. Compared to bare SC films, porosity decreases by 68% after functionalization with TMCS, while the SC–DHDP system shows a decrease of only 13%. Treatment with functionalization agents does not significantly affect the thickness of SC films. XRR reflectograms for the ZF-based systems are shown in Figure 3B. In this case, the shift in critical angle is smaller for ZF–TMCS than for ZF–DHDP. These changes correspond to a reduction in P_A of approximately 63% for DHDP-functionalized ZF films and 27% for those treated with TMCS. These changes in P_A are not due to the volume occupied by the functional groups, but rather to the increased hydrophobicity of the films.

When performing XRR studies on bilayers, several considerations must be taken into account. If the top layer has the highest electron density (SC/ZF configuration), only its critical angle can be observed (see Supplementary Figure S5A,B). Conversely, when the top layer has a lower electron density (ZF/SC case), it is, in principle, possible to distinguish the critical angles of both layers (Supplementary Figure S5C,D). However, interference effects may hinder the precise identification of the second critical angle, making the results less reliable. Supplementary Table S1 presents the results obtained by XRR for bare and functionalized

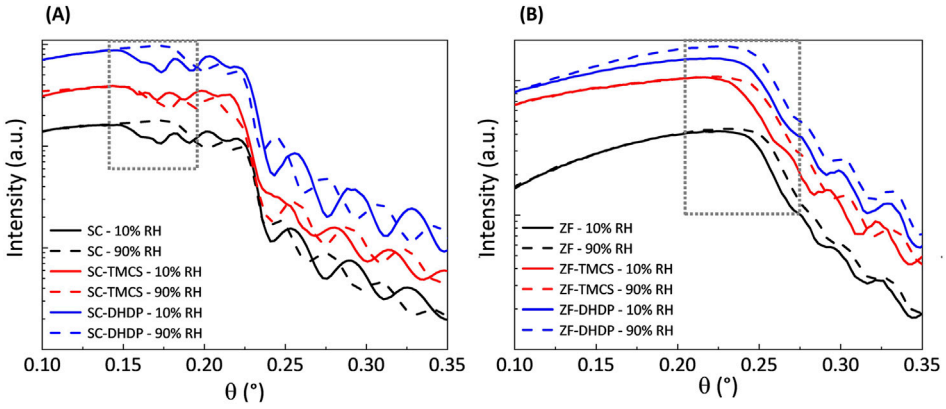

FIGURE 3
Reflectograms of SC **(A)** and ZF **(B)** systems before (black) and after functionalization with TMCS (red) or DHDP (blue), measured at 10% (solid line) and 90% (dotted line) RH. The critical angle region for both oxides is indicated with a dotted rectangle.

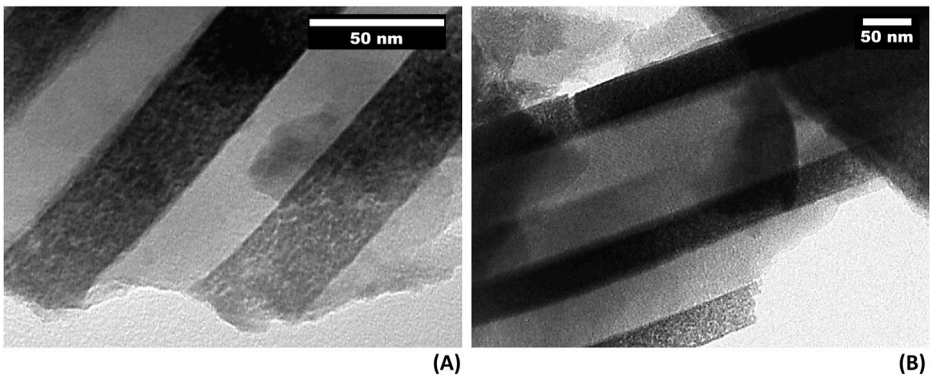

FIGURE 4
TEM image of the PC before **(A)** and after **(B)** the double functionalization (TMCS + DHDP).

bilayer systems. Consistent with the trends observed in single-layer films, the P_A of the ZF layer in the SC/ZF bilayer decreases by 15% after TMCS functionalization and by 21% after DHDP treatment. In the ZF/SC system, the SC layer exhibits a 63% reduction in P_A following TMCS functionalization, while DHDP treatment leads to a slight increase. For the ZF layer in this configuration, the critical angle could not be reliably identified, and thus, changes in P_A could not be quantified.

Multilayers characterization

TEM images of the multilayers presented in Figure 4; Supplementary Figure S7. Since Zr has a higher electron scattering cross-section than Si, the ZF layers appear as dark stripes in the images, while SC layers appear lighter. Layer thicknesses are very uniform, as shown in our previous studies of multilayer structures fabricated using similar methods (Fuertes et al., 2007; Sansierra et al., 2019; Morrone et al., 2021). Typical roughness

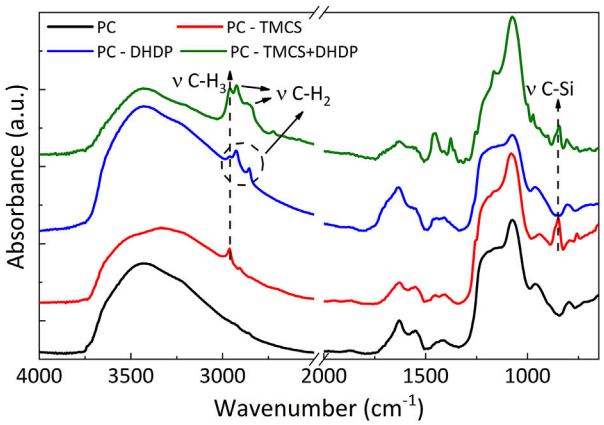

FIGURE 5
DRIFTS spectra for PC without functions (black), and functionalized with TMCS (red), DHDP (blue), and with the double modification TMCS + DHDP (green).

is below 2 nm. The mesopores are visible within the stripes as brighter regions. The images reveal well-defined stacked SC and ZF layers, with no evidence of interpenetration between the materials. Additionally, no film cracking is observed.

For all layers, the thicknesses estimated from the TEM images are approximately (40 ± 8) nm, which corresponds to the target values for constructing PCs with a band gap in the UV region using this combination of porous oxides. After sequential functionalization with TMCS and DHDP, the layered structure remains intact. In fact, the micrograph of the PC-TMCS + DHDP sample shows no significant changes in layers' thicknesses or porosities compared to the unmodified PC (see Figure 4).

The incorporation of surface chemical modifications was studied by EDS and infrared spectroscopy. Figure 5 shows the DRIFTS spectra of the multilayer system before functionalization, after treatment with TMCS or DHDP, and after sequential functionalization with both reagents. Upon reaction with TMCS, a new absorption band appears at 850 cm^{-1}, corresponding to the ν_{Si-C} vibrations characteristic of the trimethylsilyl group. Additionally, a band at 2,960 cm^{-1} is observed, associated with the ν_{C-H} stretching vibrations of CH_3 groups. These features confirm the successful surface modification of the mesoporous PC. Notably, this latter band is not detected in single- or bilayer systems, likely because the multilayer system contains four stacked layers, increasing the overall signal intensity. For DHDP functionalization, the appearance of ν_{C-H} stretching bands characteristic of alkyl chains is observed in the 2,800–3000 cm^{-1} region. After further modification of the PC–TMCS sample with DHDP, the 2,960 cm^{-1} band overlaps with the DHDP signals in this region. The simultaneous presence of all these bands confirms the successful incorporation of both functionalizing agents.

To confirm the penetration of DHDP within the multilayer structure, additional FTIR measurements in transmission mode were performed on single layers, bilayers, and multilayers deposited on glass or fused silica substrates (Supplementary Figure S6). The results show that, when normalizing by the layer's thicknesses, the amount of DHDP incorporated into the 8-layered device (containing 4 ZF layers) is nearly three times higher than that observed for a single ZF layer. This indicates that DHDP molecules infiltrate nearly all the entire accessible pore volume. However, the total DHDP content in the multilayer is slightly lower than the theoretical maximum (assuming all ZF layers were filled to the same extent as a single layer) likely due to diffusion limitations within the more complex multilayer architecture. As the upper layers begin adsorbing DHDP, the accessibility of deeper ZF layers decreases, making it progressively more difficult for DHDP to diffuse and reach the bottom layers.

Once the presence of the organic functions throughout the entire PC was confirmed, the specificity of the functionalization was addressed. To this end, EDS spectra were acquired coupled with TEM imaging. Spectra from specific regions of the PCs before and after functionalization were obtained, as shown in Supplementary Figure S7. The incorporation of DHDP can, in principle, be tracked by detecting phosphorus. However, in these samples, the presence of P in ZF layers could not be unambiguously identified due to the overlap between the K-α line of P and the L-α line of Zr, combined with the relatively low P content compared to Zr. Nevertheless, no P signal was detected in the SC layers after functionalization. Since the presence of DHDP was independently confirmed by infrared spectroscopy, it can be concluded that this molecule is specifically attached to the ZF layers. Unfortunately, due to the resolution limits of EDS and the small thickness of the ZF layers, isolated spectra of individual layers could not be obtained. As a result, silicon appears in both functionalized and non-functionalized samples, preventing the confirmation of TCMS functionalization specificity by this technique.

TABLE 3 Contact angle values of 4X (SC/ZF) multilayer before and after functionalization.

CA/°			
PC	PC-TMCS	PC-DHDP	PC-TMCS + DHDP
52 ± 4	58 ± 4	75 ± 5	69 ± 5

Subsequently, the surface physicochemical properties were evaluated through CA measurements (Table 3). The non-functionalized multilayer exhibits a higher CA (52°) than the single-layer films. This is expected, as the thicker porous PC is less polarizable than the glass substrate, which lies closer to the fluid–air–solid interface in single-layer systems. Functionalization of the PC with TMCS does not result in a significant change in the CA. In contrast, derivatization with DHDP leads to a 44% increase in CA. These results are consistent with the fact that the topmost layer is ZF, which reacts selectively with DHDP. Finally, when the PC is sequentially functionalized with both TMCS and DHDP (PC–TMCS + DHDP system), the resulting CA is comparable to that of the PC–DHDP system. Thus, the hydrophobicity of the multilayer system can be enhanced through appropriate surface functionalization, thereby improving the selectivity of the device.

Finally, the devices' optical behavior was evaluated. The as-prepared multilayer exhibits a photonic band gap centered at λ_B = 270 nm, with an average full width at half maximum of approximately 100 nm and a maximum reflectance close to 90% at λ_B, as can be seen in Figure 6. This remarkably high reflectivity is achieved with only 8 layers, owing to the high refractive index contrast between the oxides. A precise determination of the band gap width is limited by the onset of UV absorption below 225 nm from the constituent materials of the PC. All systems retain their photonic band gap after functionalization, with no changes in either the central wavelength or the bandwidth. The minor differences in λ_B values observed among all the dry PCs are similar to those found when sampling different areas of the same PC and are attributed to minor thickness variations inherent to the synthesis method. Therefore, to compare the response of these different PCs to vapors, the total displacement of the band gap position ($\Delta\lambda_B$) is analyzed rather than the absolute initial and final value of λ_B.

Sensing performance

The optical response of the PCs to different analytes was evaluated using transmission UV-Vis spectroscopy in controlled atmosphere. Spectra were acquired under dry conditions and in atmosphere saturated with the vapors of different solvents. Measurements were performed both at equilibrium conditions and dynamically, to elucidate the response kinetics. In

10.3389/fnano.2025.1631560

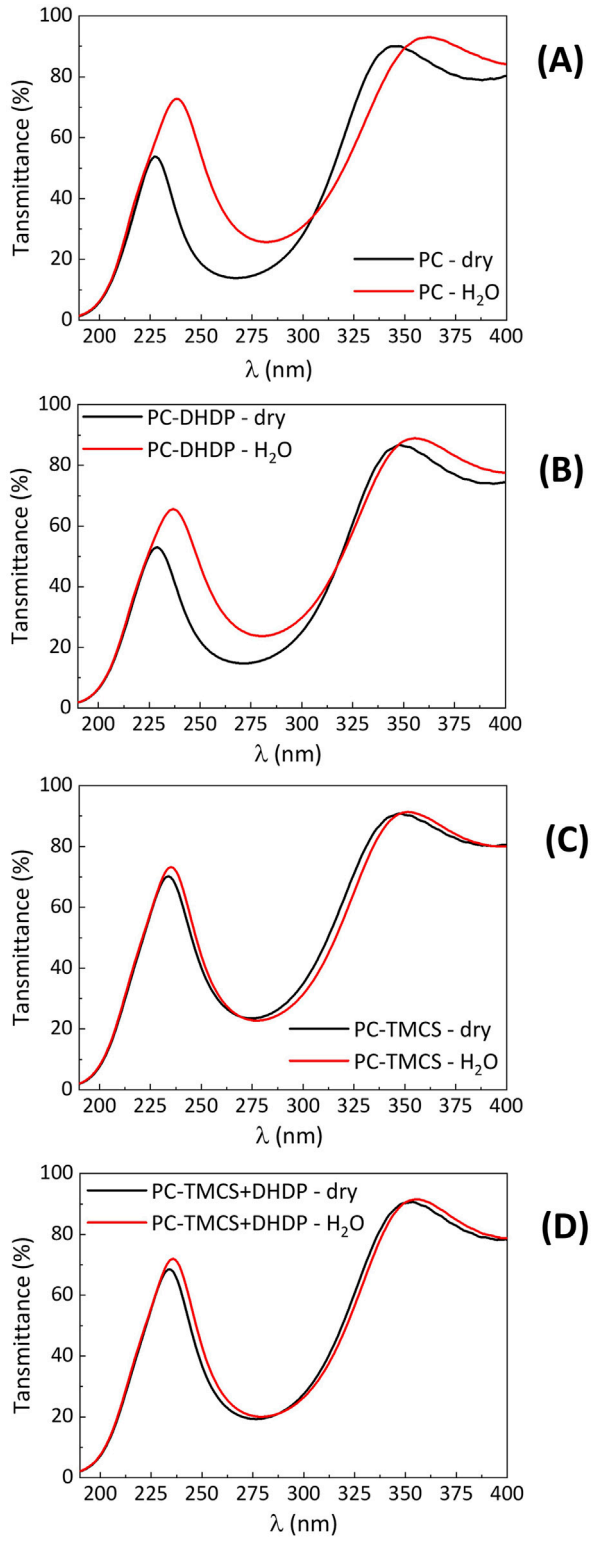

FIGURE 6
UV-visible spectra in transmission mode of 4X (SC/ZF) multilayer with and without functions, dry (black line), and exposed to water vapor (red line). **(A)** PC; **(B)** PC -TMCS; **(C)** PC-DHDP; **(D)** PC-TMCS + DHDP.

equilibrium experiments, the partial pressure of each solvent corresponds to its equilibrium P_v at the studied temperature (55 °C for all experiments). In the dynamic experiments, the partial pressure of the solvent gradually increases until it reaches the equilibrium value.

First, the water uptake in the different devices was determined. The results are presented in Figure 6 and Supplementary Table S2, SI. Upon exposure to water vapor, the non-functionalized 4X (SC/ZF) system is responsive, and the photonic band gap shift is approximately 16 nm. After derivatization, the systems remain responsive; however, the shift of λ_B upon water vapor exposure is significantly reduced. In systems functionalized only with DHDP, the λ_B shift decreases by about 50% compared to the non-functionalized PC. In contrast, systems modified with TMCS, either alone or in combination with DHDP, exhibit an even more pronounced reduction, with the λ_B shift diminishing by approximately 90%.

Therefore, functionalization has a marked effect on water condensation within the films. DHDP limits water condensation, presumably within the ZF layers, restricting it mainly to the SC layers. This partial condensation leads to a reduced refractive index contrast and an increase in the average refractive index, resulting in a redshift of the band gap and a decrease in reflectivity. In contrast, functionalization with TMCS produces a much stronger effect, significantly limiting water condensation and resulting in minimal band gap shifts.

Capillary condensation in mesopores can be understood using the Kelvin equation (Boissiere et al., 2005; Butt and Kappl, 2010). The equilibrium vapor pressure of a liquid condensed in a pore is governed by the curvature of the meniscus formed. This curvature is determined by the characteristic pore size and by the contact angle of the liquid-solid interface. Therefore, liquids will condense at lower partial pressures on smaller pores and more wettable surfaces than in larger pores and surfaces that show less favorable interactions with the condensing phase (see Supplementary Figure S8).

ZF layers have a larger pore size than SC layers, as previously described; therefore, SC pores are expected to fill with liquid water at a lower water partial vapor pressure (Fuertes et al., 2008). After functionalization with DHDP, the surface wettability of ZF layers decreases, producing a synergistic effect with pore size that enhances the differences between both layers. As a result, water condenses preferentially in SC layers, while capillary condensation does not occur in the non-wetting, functionalized ZF layers. In contrast, functionalization with TMCS has an antagonistic effect relative to pore size, as the layers with smaller pores now exhibit non-wetting behavior. Furthermore, the contact angle on ZF surfaces is also affected by dehydration, as previously discussed, effectively preventing pore filling.

Overall, the obtained results indicate that the incorporation of the tested functional groups prevents water condensation and, consequently, may render the PC response more resilient to ambient humidity. Thus, once the water uptake behavior under equilibrium conditions was determined, the dynamic optical response of the different multilayer systems to water and two non-polar organic vapors was evaluated. The PCs were exposed to atmospheres containing water, toluene, or benzyl alcohol vapors, and UV-Vis transmission spectra were recorded at regular intervals. The results are presented in Figure 7 and Table 4.

First, the response times were compared, revealing clear differences depending on the solvent used. Notably, the response to all vapors was very fast before the chemical modification: the maximum photonic band shift occurred in under 2 min. After the

10.3389/fnano.2025.1631560

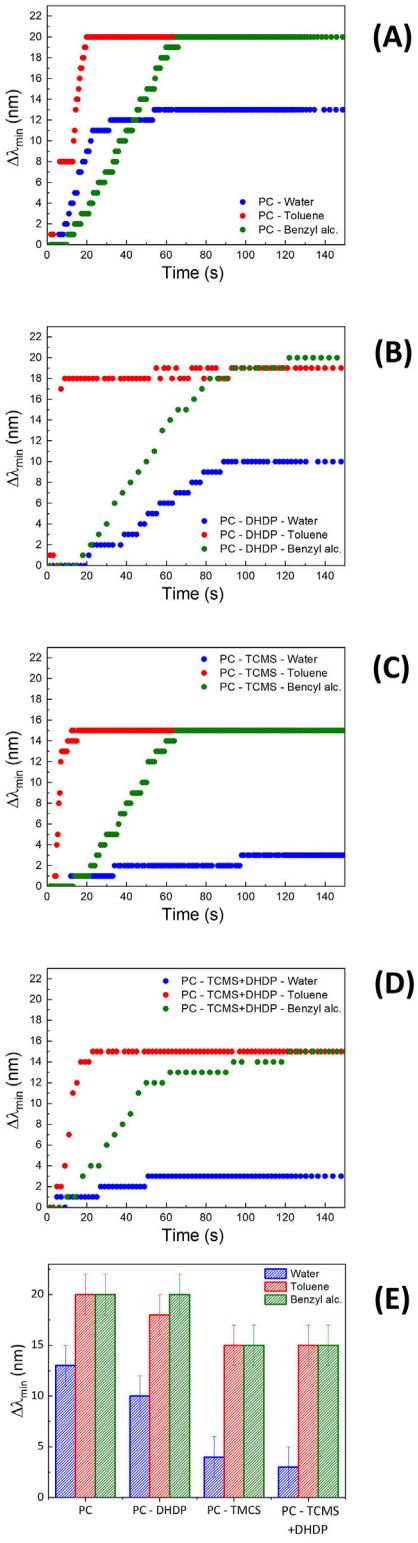

FIGURE 7
Displacement of the photonic band gap for each system exposed to the different solvents as a function of the time in contact with the vapors: **(A)** PC, **(B)** PC - DHDP, **(C)** PC - TCMS and **(D)** PC - TCMS + DHDP. **(E)** Shift of the photonic band gap measured after 2 min of exposure to each solvent, once equilibrium is reached.

TABLE 4 Response times for the devices evaluated for vapor sensing. The error in each measurement is around 10%.

System	Response time/s		
	Water	Toluene	Benzyl alcohol
PC	54	20	66
PC-TMCS	-	9	66
PC-DHDP	89	9	122
PC-TMCS + DHDP	-	23	122

functionalization, responses times as short as 9 s were measured for toluene. In the case of exposure to water vapor, the PC-DHDP system showed a 65% increase in response time compared to the non-functionalized PC while for TMCS-functionalized system the response was undetectable due to the significantly reduced accessibility of water molecules to the multilayered structure. Nevertheless, the functionalized multilayers remained responsive to toluene and benzyl alcohol vapors, confirming that the chemical modifications did not block the pores and that the porosity remained accessible.

When comparing the two organic solvents, the response to toluene was consistently faster than to benzyl alcohol (see Table 4). Upon exposure to toluene vapors, all systems exhibit very short response times (around 10–20 s). In contrast, exposure to benzyl alcohol results in response time between 1 and 2 min, depending on the functionalization. Since the optical response in these mesoporous systems originates from capillary condensation within the pores, the characteristic response time is associated with the time required for the solvent's partial pressure inside the pores to reach the threshold for capillary condensation. From the solvent perspective, lower P_v and higher molecular weight reduce diffusion rates, also extending the time required for condensation: this is the case of benzyl alcohol compared to toluene. This behavior is consistent with previous observations in mesoporous multilayer systems based on titania and silica films with photonic response in the visible region of the spectrum (Sansierra et al., 2019).

Besides, from the perspective of the porous material, less wettable surfaces (as can be obtained using the functionalization agents) and larger pore diameters (in these multilayers, in the ZF layers) demand a higher partial pressure for condensation, thus requiring longer times to complete the filling with the solvent.

After functionalization with DHDP, the strong interactions between the alcohol group of the benzyl alcohol and the ZrO_2 surface are replaced by weaker interactions with the aliphatic chains of the phosphate. As a result, higher solvent partial pressures are required to trigger capillary condensation, leading to longer response times: from 1 to 2 min.

By the other hand, TMCS reacts selectively with the SC films, which have smaller pore sizes and therefore require lower partial pressures for condensation; in this case, the changes in surface wettability are not sufficient to outweigh the pore size effect. Therefore, the observed difference in the time response between

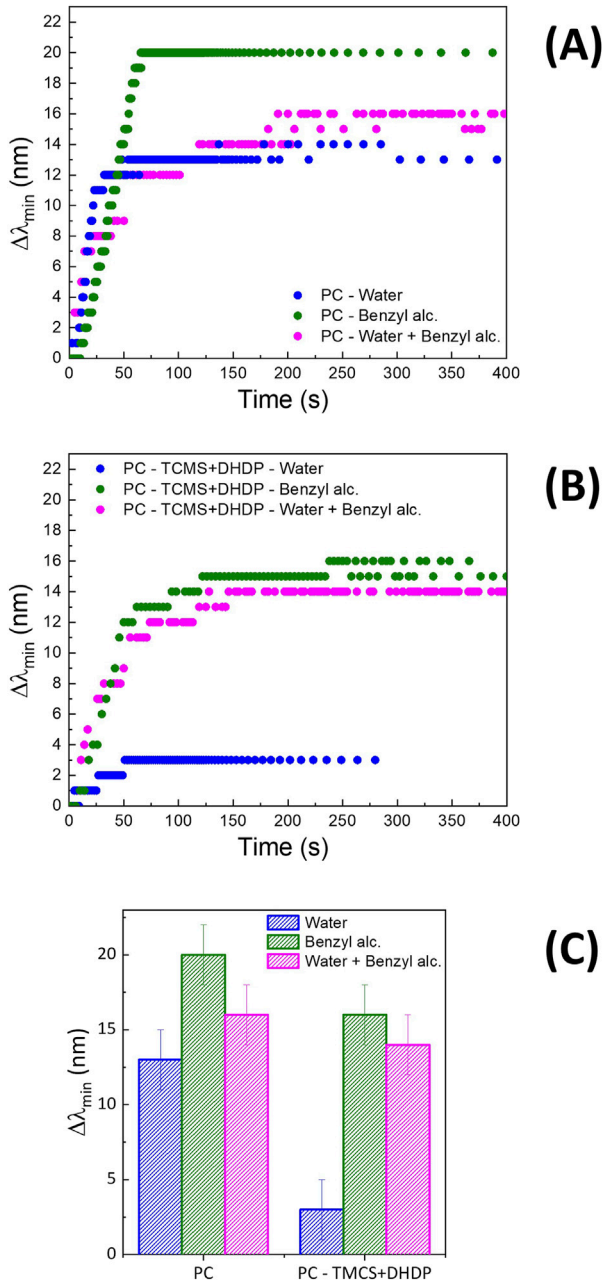

FIGURE 8
Displacement of the photonic band gap for the PC before and after double functionalization, upon exposure to the pure solvents (water or benzyl alcohol) or a mixture of solvents (water + benzyl alcohol), as a function of the time in contact with the vapors: **(A)** PC, **(B)** PC-TMCS + DHDP. **(C)** Shift of the photonic band gap measured once equilibrium is reached.

benzyl alcohol and toluene detected using both modified PCs can be attributed to the presence of the interaction between the DHDP and the hydroxyl group in benzyl alcohol.

It is noteworthy that the maximum shifts of the photonic band gap for both organic solvents are equivalent for each device (Figure 7E). These solvents exhibit similar refractive indices and thus produce comparable photonic band shifts in this type of optical device (Sansierra et al., 2019).

After analyzing the behavior of the devices detecting the pure solvents, the dynamic displacement of the photonic band gap in a mixture of solvents was studied. These tests aimed to evaluate the PCs responsiveness in a mixed vapor environment, simulating the detection of a non-polar organic compound under high humidity conditions. The results obtained for the mixture of water and benzyl alcohol are presented in Figure 8.

First, the change in the optical properties of the dry non-functionalized PC exposed to an atmosphere containing both water and benzyl alcohol vapors is shown in Figure 8A. During the initial seconds, the system responds predominantly to water, given its higher P_v, resulting in a behavior similar to that observed under pure water vapor. As the environment becomes saturated with benzyl alcohol (approximately after 20 s), the solvents adsorption dynamics change slightly. Nevertheless, the final shift in the photonic band gap is close to that obtained under pure water vapor. This indicates that, in the absence of surface functionalization, the presence of water in the environment diminishes the photonic crystal's response to benzyl alcohol vapors compared to the response observed under pure benzyl alcohol.

The same experiment was then performed using the double-functionalized PC (Figure 8B). In this case, the optical response in the mixed solvent environment closely resembles that observed under exposure to the pure non-polar solvent. The amount of water condensed within the functionalized PC is minimal, allowing benzyl alcohol to be detected within just a few seconds from the start of the experiment. Notably, the presence of water vapor in the atmosphere does not hinder the detection of the non-polar solvent, even though benzyl alcohol has a lower P_v than water.

Figure 8C shows the shift of the photonic band gap measured once equilibrium is reached for both pure vapors and their mixture, comparing non-functionalized and functionalized PCs. For the solvents mixture, the maximum shift is slightly lower than that observed with pure benzyl alcohol. This reduction is attributed to the presence of a small amount of condensed water, which has a lower refractive index than the non-polar solvent.

A similar behavior was observed for the water-toluene mixture, as shown in Supplementary Figure S9. In this case, both solvents exhibit comparable vapor pressures, further supporting the conclusion that water does not interfere with the detection of non-polar solvents in this type of functionalized detectors.

Finally, these UV optical devices showed excellent chemical and mechanical robustness. Each one was tested several times (at least 40) under different conditions, and consistently delivered reliable results without any observable damage or loss of function. This highlights a clear advantage of using mesoporous oxides in their construction: their strong resistance to chemical and mechanical stress (Sansierra et al., 2019; Ramallo et al., 2022). Furthermore, even after repeated use, the devices maintained a fully reversible optical response simply by drying them in an oven at 130 °C for 15 min between exposures to different solvents. This makes them especially promising for long-term use in UV sensing applications, where stability, durability and UV resistance are critical.

Conclusions

In this work, the chemical differences between silicon and zirconium oxides were exploited to obtain high-reflectivity porous photonic crystals with a photonic band gap in the UV, whose response to polar and non-polar vapors can be controlled.

In a first step, the specific functionalization of single layers and bilayers based on mesoporous SiO_2 and ZrO_2 was studied. Trimethylchlorosilane was employed to modify the SiO_2 surface, while dihexadecylphosphate was used to functionalize the ZrO_2 surface. The selectivity of this procedure arises from the greater hydrolytic stability of Zr–O–P and Si–O–Si bonds compared to Zr–O–Si and Si–O–P linkages. The success of this strategy was confirmed by IR spectroscopy, which revealed distinctive signals corresponding to each organic group on its respective oxide, but not on the other.

Afterwards, photonic crystals were built, by alternate deposition of mesoporous zirconia and silica. These devices proved to be robust and stable, exhibiting a reversible optical response upon exposure to polar and non-polar vapors, in the UV region. These PC were subjected to the same functionalization strategy used for the single oxides, taking into account that successive reaction steps were required. By means of infrared spectroscopy, it was demonstrated that the functionalization of the PC occurred along the whole multilayered structure. EDS measurements coupled to TEM and DRIFTS, on the other hand, indicated that the specific functionalization observed for single layers is also possible in the PCs. The chemical modifications performed after the PCs construction preserved the optical properties and responsiveness of the devices. Besides, water condensation inside the mesoporous structure was clearly reduced after functionalization, highlighting this approach as a promising strategy for developing detectors that are minimally sensitive to ambient humidity while remaining responsive to non-polar substances in the vapor phase.

The functionalization strategy developed in this work can be readily extended to other responsive photonic devices. This is especially relevant for systems with alternating layers of silica and transition metal oxides, given the strong affinity of organic phosphates for metal oxide surfaces. By allowing the incorporation of specific chemical functions into targeted layers without altering the structural or optical properties of the films, this methodology offers new opportunities for the rational design of multifunctional sensing platforms. Moreover, the fact that the band gap of the developed PCs is located in the UV region of the spectrum could be exploited to combine these systems with other sensing devices that work in the visible region, without overlapping the functioning of each component. Consequently, the specific functionalization strategy, combined with a UV-centered photonic band gap, paves the way for the development of advanced detector arrays and photonic noses capable of distinguishing complex analyte mixtures through differential optical responses (Bonifacio et al., 2010; Bonifacio et al., 2011; Kelly et al., 2011; Däntl et al., 2022; Wei et al., 2024).

Data availability statement

The raw data supporting the conclusions of this article will be made available by the authors upon reasonable request.

Author contributions

JM: Investigation, Visualization, Writing – original draft, Writing – review and editing. PCA: Conceptualization, Visualization, Funding acquisition, Writing – review and editing. AZ: Conceptualization, Supervision, Visualization, Funding acquisition, Writing – original draft, Writing – review and editing. MCF: Conceptualization, Supervision, Visualization, Funding acquisition, Writing – original draft, Writing – review and editing.

Funding

The author(s) declare that financial support was received for the research and/or publication of this article. This work was supported by Agencia I + D + i (projects PICT 2021-I-A-00495 and PICT 2021-CAT-II-00062) and CONICET (PIP 11220210100158CO).

Acknowledgments

The authors thank G. Zbihlei (CAC-CNEA) for the TEM images and the EDS measurements. The authors especially thank the reviewers for their critical corrections and valuable suggestions, which have significantly contributed to improving this work.

Conflict of interest

The authors declare that the research was conducted in the absence of any commercial or financial relationships that could be construed as a potential conflict of interest.

Generative AI statement

The author(s) declare that no Generative AI was used in the creation of this manuscript.

Publisher's note

Supplementary material

The Supplementary Material for this article can be found online at: https://www.frontiersin.org/articles/10.3389/fnano.2025.1631560/full#supplementary-material

References

Angelomé, P. C., and Soler-Illia, G. J. A. A. (2005). Organically modified transition-metal oxide mesoporous thin films and xerogels. *Chem. Mater.* 17 (2), 322–331. doi:10.1021/cm048559b

Athens, G. L., Shayib, R. M., and Chmelka, B. F. (2009). Functionalization of mesostructured inorganic–organic and porous inorganic materials. *Curr. Opin. Colloid and Interface Sci.* 14 (4), 281–292. doi:10.1016/j.cocis.2009.05.012

Boissiere, C., Grosso, D., Lepoutre, S., Nicole, L., Bruneau, A. B., and Sanchez, C. (2005). Porosity and mechanical properties of mesoporous thin films assessed by environmental ellipsometric porosimetry. *Langmuir* 21 (26), 12362–12371. doi:10.1021/la050981z

Bonifacio, L. D., Ozin, G. A., and Arsenault, A. C. (2011). Photonic nose–sensor platform for water and food quality control. *Small* 7 (22), 3153–3157. doi:10.1002/smll.201101074

Bonifacio, L. D., Puzzo, D. P., Breslav, S., Willey, B. M., McGeer, A., and Ozin, G. A. (2010). Towards the photonic nose: a novel platform for molecule and bacteria identification. *Adv. Mater.* 22 (12), 1351–1354. doi:10.1002/adma.200902763

Brinker, C. J., Lu, Y., Sellinger, A., and Fan, H. (1999). Evaporation-induced self-assembly: nanostructures made easy. *Adv. Mater.* 11 (7), 579–585. doi:10.1002/(sici)1521-4095(199905)11:7<579::aid-adma579>3.0.co;2-r

Burgess, I. B., Loncar, M., and Aizenberg, J. (2013). Structural colour in colourimetric sensors and indicators. *J. Mater. Chem. C* 1 (38), 6075–6086. doi:10.1039/c3tc30919c

Butt, H.-J., and Kappl, M. (2010). "Capillary forces," in *Surface and interfacial forces*, 127–161.

Butt, M. A., and Piramidowicz, R. (2024). Integrated photonic sensors for the detection of toxic gasses—A review. *Chemosensors* 12 (7), 143. doi:10.3390/chemosensors12070143

Choi, S. Y., Mamak, M., von Freymann, G., Chopra, N., and Ozin, G. A. (2006). Mesoporous bragg stack color tunable sensors. *Nano Lett.* 6 (11), 2456–2461. doi:10.1021/nl061580m

Däntl, M., Jiménez-Solano, A., and Lotsch, B. V. (2022). Stimuli-responsive one-dimensional photonic crystals: design, fabrication and sensing. *Mater. Adv.* 3 (20), 7406–7424. doi:10.1039/D2MA00793B

Fenzl, C., Hirsch, T., and Wolfbeis, O. S. (2014). Photonic crystals for chemical sensing and biosensing. *Angew. Chem. Int. Ed.* 53 (13), 3318–3335. doi:10.1002/anie.201307828

Fuertes, M. C. (2009). Materiales funcionales multiescala basados en películas de óxidos mesoporosos. Buenos Aires, Argentina: PhD Thesis in Science and Technology of Materials, Instituto Sabato UNSAM-CNEA.

Fuertes, M. C., Colodrero, S., Lozano, G., González-Elipe, A. R., Grosso, D., Boissière, C., et al. (2008). Sorption properties of mesoporous multilayer thin films. *J. Phys. Chem. C* 112 (9), 3157–3163. doi:10.1021/jp710612y

Fuertes, M. C., López-Alcaraz, F. J., Marchi, M. C., Troiani, H. E., Luca, V., Míguez, H., et al. (2007). Photonic crystals from ordered mesoporous thin-film functional building blocks. *Adv. Funct. Mater.* 17 (8), 1247–1254. doi:10.1002/adfm.200601190

Fuertes, M. C., Marchena, M., Marchi, M. C., Wolosiuk, A., and Soler-Illia, G. J. A. A. (2009). Controlled deposition of silver nanoparticles in mesoporous Single- or multilayer thin films: from tuned pore filling to selective spatial location of nanometric objects. *Small* 5 (2), 272–280. doi:10.1002/smll.200800894

Ghazzal, M. N., Deparis, O., Errachid, A., Kebaili, H., Simonis, P., Eloy, P., et al. (2012a). Porosity control and surface sensitivity of titania/silica mesoporous multilayer coatings: applications to optical bragg resonance tuning and molecular sensing. *J. Mater. Chem.* 22 (48), 25302–25310. doi:10.1039/c2jm35107b

Ghazzal, M. N., Joseph, M., Kebaili, H., De Coninck, J., and Gaigneaux, E. M. (2012b). Tuning the selectivity and sensitivity of mesoporous dielectric multilayers by modifiying the hydrophobic–hydrophilic balance of the silica layer. *J. Mater. Chem.* 22 (42), 22526–22532. doi:10.1039/C2JM33692H

Haynes, W. N. (2003). *CRC handbook of chemistry and physics*.

Hinterholzinger, F. M., Ranft, A., Feckl, J. M., Rühle, B., Bein, T., and Lotsch, B. V. (2012). One-dimensional metal–organic framework photonic crystals used as platforms for vapor sorption. *J. Mater. Chem.* 22 (20), 10356–10362. doi:10.1039/C2JM15685G

Jeong, W., Lee, H., Hwang, Y. J., An, B., Lee, Y., Jeong, H., et al. (2025). Solution processing for colloidal nanoparticle thin film: from fundamentals to applications. *Adv. Colloid Interface Sci.* 342, 103538. doi:10.1016/j.cis.2025.103538

Joannopoulos, J. D., Johnson, S. G., Winn, J. N., and Meade, R. D. (2011). *Photonic crystals: molding the flow of light*.

Kelly, T. L., Garcia Sega, A., and Sailor, M. J. (2011). Identification and quantification of organic vapors by time-resolved diffusion in stacked mesoporous photonic crystals. *Nano Lett.* 11 (8), 3169–3173. doi:10.1021/nl201385p

Klotz, M., Rouessac, V., Rébiscoul, D., Ayral, A., and van der Lee, A. (2006). Adsorption-desorption isotherms of nanoporous thin films measured by X-ray reflectometry. *Thin Solid Films* 495, 214–218. doi:10.1016/j.tsf.2005.08.168

López-Puente, V., Angelomé, P. C., Soler-Illia, G. J. A. A., and Liz-Marzán, L. M. (2015). Selective SERS sensing modulated by functionalized mesoporous films. *ACS Appl. Mater. and Interfaces* 7 (46), 25633–25640. doi:10.1021/acsami.5b10543

Meng, Z., Liu, Y., Huang, H., and Wu, S. (2024). Flexible self-supporting photonic crystals: fabrications and responsive structural colors. *Adv. Colloid Interface Sci.* 333, 103272. doi:10.1016/j.cis.2024.103272

Morrone, J., Ramallo, J. I., Boissière, C., Angelomé, P. C., and Fuertes, M. C. (2023). Effect of aqueous media over stability and optical performance of mesoporous 1D photonic crystals. *Chem. Mater.* 35 (21), 8897–8908. doi:10.1021/acs.chemmater.3c01343

Morrone, J., Ramallo, J. I., Lionello, D. F., Zelcer, A., Auguié, B., Angelomé, P. C., et al. (2021). Incorporation of porous protective layers as a strategy to improve mechanical stability of tamm plasmon based detectors. *Mater. Adv.* 2 (8), 2719–2729. doi:10.1039/D1MA00079A

Musgrove, A., Cockerham, A., Pazos, J. J., Shahriar, S., McMahon, M., Touma, J. E., et al. (2024). Bio-inspired photonic and plasmonic systems for gas sensing: applications, fabrication, and analytical methods. *J. Opt. Microsystems* 4 (2), 020902. doi:10.1117/1.jom.4.2.020902

Nicole, L., Boissiere, C., Grosso, D., Quach, A., and Sanchez, C. (2005). Mesostructured hybrid organic-inorganic thin films. *J. Mater. Chem.* 15 (35-36), 3598–3627. doi:10.1039/B506072A

Paternò, G. M., Moscardi, L., Donini, S., Ariodanti, D., Kriegel, I., Zani, M., et al. (2019). Hybrid one-dimensional plasmonic–photonic crystals for optical detection of bacterial contaminants. *J. Phys. Chem. Lett.* 10 (17), 4980–4986. doi:10.1021/acs.jpclett.9b01612

Ramallo, J. I., Morrone, J., Lionello, D. F., Angelomé, P. C., and Fuertes, M. C. (2022). Mechanical properties and structural integrity of devices based on sol–gel mesoporous oxides thin films. *J. Sol-Gel Sci. Technol.* 102 (1), 185–196. doi:10.1007/s10971-021-05636-5

Sansierra, M. C., Morrone, J., Cornacchiulo, F., Fuertes, M. C., and Angelomé, P. C. (2019). Detection of organic vapors using tamm mode based devices built from mesoporous oxide thin films. *ChemNanoMat* 5 (10), 1289–1295. doi:10.1002/cnma.201900388

Sienko, M. J., and Plane, R. A. (1967). *Química*. Spain: Editorial Aguilar.

Shen, Y., Tissot, A., and Serre, C. (2022). Recent progress on MOF-Based optical sensors for VOC sensing. *Chem. Sci.* 13 (47), 13978–14007. doi:10.1039/D2SC04314A

Steinberg, P. Y., Zalduendo, M. M., Giménez, G., Soler-Illia, G. J. A. A., and Angelomé, P. C. (2019). TiO2 mesoporous thin film architecture as a tool to control Au nanoparticles growth and sensing capabilities. *Phys. Chem. Chem. Phys.* 21 (20), 10347–10356. doi:10.1039/C9CP01896D

Sun, L.-N., Lu, L.-X., Pan, L., Lu, L.-J., and Qiu, X.-L. (2021). Development of active low-density polyethylene (LDPE) antioxidant packaging films: controlled release effect of modified mesoporous silicas. *Food Packag. Shelf Life* 27, 100616. doi:10.1016/j.fpsl.2020.100616

van der Lee, A. (2000). Grazing incidence specular reflectivity: theory, experiment, and applications. *Solid State Sci.* 2 (2), 257–278. doi:10.1016/s1293-2558(00)00119-9

Venkateswara Rao, A., Latthe, S. S., Nadargi, D. Y., Hirashima, H., and Ganesan, V. (2009). Preparation of MTMS based transparent superhydrophobic silica films by sol–gel method. *J. Colloid Interface Sci.* 332 (2), 484–490. doi:10.1016/j.jcis.2009.01.012

Wang, Z., Wang, Y., Yan, J., Liu, B., Chen, Y., and Tian, Y. (2022). Metal–organic framework-based photonic crystal platforms for gas sensing: a review. *Mater. Adv.* 3 (17), 6728–6741. doi:10.1039/D2MA00269H

Wei, J., Yi, Z., Yang, L., Zhang, L., Yang, J., Qin, M., et al. (2024). Photonic crystal gas sensors based on metal–organic frameworks and polymers. *Anal. Methods* 16 (29), 4901–4916. doi:10.1039/D4AY00764F

Xu, H., Wu, P., Zhu, C., Elbaz, A., and Gu, Z. Z. (2013). Photonic crystal for gas sensing. *J. Mater. Chem. C* 1 (38), 6087–6098. doi:10.1039/C3TC30722K

Zelcer, A., and Soler-Illia, G. J. A. A. (2013). One-step preparation of UV transparent highly ordered mesoporous zirconia thin films. *J. Mater. Chem. C* 1 (7), 1359–1367. doi:10.1039/c2tc00319h

Zhao, X. S., and Lu, G. Q. (1998). Modification of MCM-41 by surface silylation with trimethylchlorosilane and adsorption study. *J. Phys. Chem. B* 102 (9), 1556–1561. doi:10.1021/jp972788m